International Journal of Robotics and Control Systems
Vol. 5, No. 5, 2025, pp. 2750-2766
ISSN 2775-2658
http://pubs2.ascee.org/index.php/ijrcs

Fuzzy Logic–Based Control with MPPT for Power Quality Enhancement in DFIG Wind Energy Systems

Fatima-Ezzahra Blouh [a,1,*], Mohamed Bezza [a,2], Abdelfatah El Azzab [b,3]

[a] LSIB Laboratory, FST of Mohammedia, Hassan II University of Casablanca, Morocco
[b] EEIS Laboratory, FST of Mohammedia, Hassan II University of Casablanca, Morocco
[1] blfatimaezzahra2016@gmail.com; [2] mohamed.bezza@fstm.ac.ma; [3] elazzab.abdelfattah96@gmail.com
[*] Corresponding Author

ARTICLE INFO

Article history
Received September 02, 2025
Revised November 04, 2025
Accepted November 27, 2025

Keywords
Wind Energy;
DFIG;
Back-to-Back Converter;
Rotor-Side Converter;
Grid-Side Converter;
Fuzzy Logic Control;
MPPT (Perturb and Observe);
Power Quality

ABSTRACT

This paper explores the control challenges in wind energy conversion systems (WECS) that use a doubly fed induction generator (DFIG) combined with advanced power converters, aiming to enhance power quality and dynamic performance. Indeed, the proposed control technique based on fuzzy logic controller (FLC) is developed to enhance overall performance of the studied system. The back-to-back converter technology allows bidirectional power flow and enhances the waveform quality and ensuring efficient energy conversion. To extract the maximum power from the wind turbine, we use a perturb and observe (P&O)-based maximum power point tracking (MPPT) algorithm. The system is modeled in the dq-reference frame and tested under both step-change and random wind speed profiles. MATLAB/Simulink results demonstrate that the proposed control strategy effectively maintains system stability and significantly improves power quality under varying wind conditions.

1. Introduction

As the world faces the depletion of fossil fuel resources, the urgency for sustainable and renewable energy solutions has never been greater. Reliance on coal- and gas-fired power plants is increasingly seen as unsustainable, prompting a global shift toward cleaner and more efficient energy systems [1], [2]. Within this landscape, wind power has emerged as a cornerstone of the energy transition due to its cost-effectiveness and low carbon footprint. Substantial investments worldwide have been channeled into developing large-scale wind farms, making the Wind Energy Conversion System (WECS) a critical area of research [3]-[5].

Among the various renewable energy options, wind energy has emerged as a particularly promising source for distributed generation and is increasingly integrated into modern power systems [6], [7]. At the heart of this transition is the DFIG, widely recognized as one of the most efficient and versatile variable-speed generators for wind turbine applications. The DFIG's flexibility brings several advantages, including variable-speed operation, independent control of active and reactive power, and high-power conversion efficiency [8], [9]. Some designs even support direct-drive operation, eliminating the need for a gearbox, which reduces maintenance requirements and enhances reliability. These characteristics make the DFIG an excellent choice for large-scale wind power plants

(WPPs), often exceeding one megawatt in capacity, while also meeting the increasing demand for advanced voltage and current control in both domestic and international energy markets [10], [11].

In DFIG-based wind energy conversion systems, the power converter is a key component that directly influences both energy capture and grid integration performance [12]. The widely adopted back-to-back converter topology consists of two main stages: the rotor-side converter (RSC) and the grid-side converter (GSC) [13]. The RSC governs the exchange of power between the rotor and the converter, enabling variable-speed operation and ensuring that the DFIG extracts maximum power under fluctuating wind conditions. Complementing this, the GSC manages the energy transfer between the DFIG and the electrical grid, maintaining voltage and frequency stability while enabling independent control of active and reactive power [14], [15]. By facilitating bidirectional power flow and precise control of electrical parameters, the combined operation of the RSC and GSC not only optimizes turbine efficiency but also enhances the ability of wind power plants to meet grid code requirements and contribute to overall system stability [16]. A fundamental advantage of the DFIG lies in its flexible control capabilities, which are achieved through coordinated operation of the RSC and GSC. The RSC is typically controlled to regulate rotor currents while the GSC ensures a stable DC-link voltage and adjusts reactive power exchange with the grid.

Recent research on DFIG-based wind energy conversion systems has explored a variety of advanced control strategies aimed at improving dynamic performance, reducing power ripples, and enhancing robustness under varying operating conditions. In [17], an intelligent metaheuristics-based approach was proposed for tuning PI controllers in a direct power control scheme, employing the Thermal Exchange Optimization (TEO) algorithm to outperform other well-known metaheuristics in tracking and control accuracy. In [18], an improved active and reactive power extraction method for variable-speed dual-rotor wind power systems used a direct vector control scheme with fuzzy PWM and neural PI control. The work in [19] introduced a Modified Super Twisting (MST) algorithm based on second-order sliding mode control for grid-connected DFIGs. Similarly, [20] compared vector and linear control strategies for wind turbines connected to a DC collector grid, highlighting the trade-offs in performance under varying operating modes. An improved DPC method without a phase-locked loop (PLL) was presented in [21], simplifying implementation by transforming time-varying dynamics into constant coefficients for easier linear control. In addition, advanced control strategies have been proposed to improve the performance of WECS based on PMSG, in [22]-[24], a Higher Order Sliding Mode Controller combined with a Disturbance Observer and a Modified Super-Twisting Integral Terminal Sliding Mode Control (MSTIFTSMC) approach was developed to ensure MPPT and enhance power quality under complex operating conditions. In [25], a direct power synergetic-sliding mode control was developed to maintain constant switching frequency and minimize ripples in reactive power, torque, and current, while [26] proposed a hybrid adaptive backstepping–sliding mode control to cancel chattering and improve power control precision. Further advancements include the integration of fractional calculus theory with the super-twisting algorithm (STA) for asynchronous generator systems [27], yielding substantial THD and ripple reduction, and the use of a fractional-order PI super-twisting sliding mode controller (FOPI-STSMC) [28] to reduce chattering and improve robustness compared to conventional sliding mode control. Finally, [29] proposed a neural direct power control method combining four-level neural space vector PWM (4L-NSVPWM) with neural PI controllers. These advancements demonstrate substantial progress in enhancing DFIG control, yet they highlight trade-offs among robustness, complexity, parameter sensitivity, and power quality, suggesting opportunities for alternative approaches that better balance these objectives. Although these methods have significantly improved control performance, most suffer from inherent drawbacks such as high computational complexity, sensitivity to parameter variations, and the need for extensive tuning. In contrast, FLC offer a simpler but powerful alternative, capable of handling system nonlinearities and uncertainties without requiring a precise mathematical model.

This work proposes an advanced control framework for wind energy conversion systems employing a DFIG (Fig. 1), with a particular emphasis on improving power quality and operational

stability. The approach combines a back-to-back converter with a fuzzy logic controller, where the converter ensures bidirectional power flow and high-quality waveforms, while the FLC provides robust and adaptive control under fluctuating wind conditions. To further enhance energy capture, a perturb and observe (P&O)-based MPPT strategy is integrated, allowing the DFIG-based wind turbine to extract maximum power across a wide range of wind speeds. The proposed system is modeled in the dq-reference frame to facilitate accurate analysis and control design. Its performance is thoroughly assessed through MATLAB/Simulink simulations under both step-change and random wind speed profiles, demonstrating that the strategy not only guarantees system stability but also significantly enhances power quality and overall efficiency compared to conventional approaches.

In summary, this paper is organized into five main sections. We begin with an introduction (Section I) providing an overview of the study's objectives and significance. Following this, we delve into the mathematical model of DFIG-based WECS in Section II. Section III presents the control design of the studied system. In Section IV, we present the simulation results obtained from the proposed mathematical model and control design. Finally, Section V offers concluding remarks and avenues for future research.

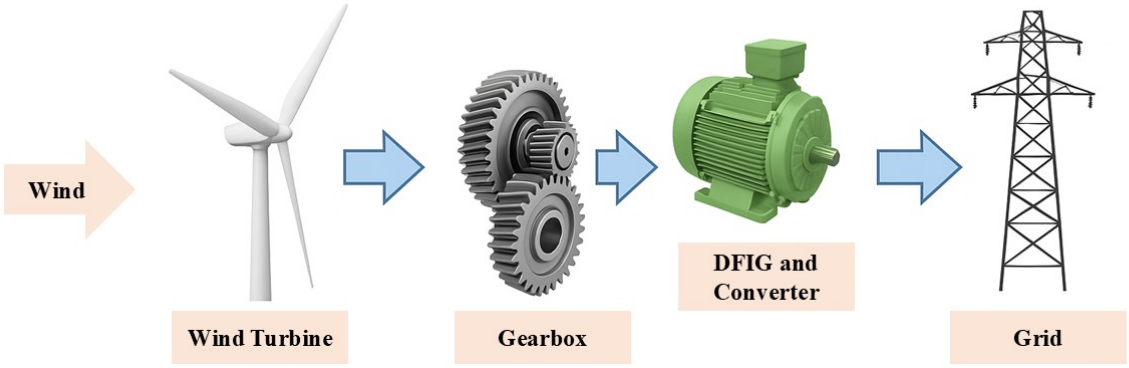

Fig. 1. Schematic representation of a DFIG-based wind energy conversion system

2. Mathematical Model of WT-Based DFIG

The wind turbine captures kinetic energy from the wind through its rotor blades and converts it into mechanical energy via the drive train. In the studied wind energy conversion system, this mechanical power is supplied to a DFIG generator, which is interfaced with the electrical grid through a back-to-back converter configuration. This arrangement enables bidirectional power flow, precise control of active and reactive power, and enhanced power quality.

2.1. Wind Turbine Modeling

The mechanical power extracted by the wind turbine can be calculated using the following relation [5], [30]:

$$P_T = \frac{1}{2}\rho C_p(\beta,\lambda)\pi R^2 V_\omega^3 \quad (1)$$

Where ρ is the air density, R is the rotor radius, V_ω is the wind speed, and $C_p(\beta,\lambda)$, is the turbine's power coefficient. The power coefficient depends on the blade pitch angle β and the tip speed ratio λ, given by:

$$\lambda = \frac{R\Omega_T}{V_\omega} \quad (2)$$

The mathematical expression of the power coefficient is defined as:

$$\begin{cases} C_p(\beta,\lambda) = c_1\left[\frac{c_2}{\lambda_l} - c_3\beta - c_4\right]e^{-\frac{c_5}{\lambda_l}} + c_6\lambda \\ \frac{1}{\lambda_l} = \frac{1}{\lambda + 0.08\beta} - \frac{0.035}{\beta^3 + 1} \end{cases} \quad (3)$$

Here, c_i $(i = 1, \ldots, 6)$ are empirical constants describing the turbine characteristics: $c_1 = 0.517, c_2 = 166, c_3 = 0.4, c_4 = 5, c_5 = 0.0068, c_6 = 0.035$.

The aerodynamic torque generated by the wind turbine is obtained from the relationship between the captured power and the rotor's angular velocity, expressed as:

$$T_T = \frac{P_T}{\Omega_T} = \frac{1}{2\Omega_T}\rho C_p(\beta,\lambda)\pi R^2 V_\omega^3 \quad (4)$$

The mechanical dynamics of the system can be described by:

$$J\frac{d\Omega_\mathrm{m}}{dt} = T_m - T_e - f\Omega_\mathrm{m} \quad (5)$$

Where J represents the total moment of inertia and f is the viscous friction coefficient.

2.2. DFIG Modeling

To maintain synchronization with the grid frequency regardless of wind speed variations, the doubly fed induction generator is modeled using the following set of equations in the rotating dq-reference frame [31]-[33]:

$$V_{ds} = R_s i_{ds} + \frac{d\phi_{ds}}{dt} - \omega_s\phi_{qs}\ ;\ V_{qs} = R_s i_{qs} + \frac{d\phi_{qs}}{dt} + \omega_s\phi_{ds} \quad (6a)$$

$$V_{dr} = R_r i_{dr} + \frac{d\phi_{dr}}{dt} - \omega_r\phi_{qr}\ ;\ V_{qr} = R_r i_{qr} + \frac{d\phi_{qr}}{dt} + \omega_r\phi_{dr} \quad (6b)$$

In these expressions, V_{ds} and V_{qs} denote the stator voltages, while V_{dr} and V_{qr}represent the rotor voltages. The variables (i_{ds}, i_{qs}) and (i_{dr}, i_{qr}) are the stator and rotor currents in the dq-frame, respectively. R_r and R_s are the stator and rotor resistances, and (ω_r, ω_s) and correspond to the stator and rotor electrical angular frequencies.

The flux linkages for the stator and rotor are given by:

$$\begin{cases} \phi_{ds} = L_s i_{ds} + M i_{dr} \\ \phi_{qs} = L_s i_{qs} + M i_{qr} \end{cases} \quad (7a)$$

$$\begin{cases} \phi_{dr} = L_r i_{dr} + M i_{ds} \\ \phi_{qr} = L_r i_{qr} + M i_{qs} \end{cases} \quad (7b)$$

Here, L_s and L_r are the self-inductances of the stator and rotor, respectively, and M is the mutual inductance.

The instantaneous active and reactive powers at the stator side are:

$$\begin{cases} P_s = V_{ds} i_{ds} + V_{qs} i_{qs} \\ Q_s = V_{qs} i_{ds} - V_{ds} i_{qs} \end{cases} \quad (8)$$

When expressed in the synchronous dqdqdq-reference frame aligned with the stator flux, the ddd-axis coincides with the stator flux vector ϕ_s. Under steady-state conditions, $V_{ds} = 0$ and $\mathrm{V}_{qs} = V_s$, leading to:

$$\begin{cases} P_s = -\dfrac{V_s M}{L_s}\, i_{qr} \\ Q_s = -\dfrac{V_s M}{L_s}\, i_{dr} + \dfrac{V_s^2}{L_s \omega_s} \end{cases} \tag{9}$$

The dynamics of the rotor currents in the dq-frame are then described by:

$$\frac{di_{dr}}{dt} = -\frac{R_r}{\Upsilon} i_{dr} + \omega_r i_{qr} + \frac{1}{\Upsilon} V_{dr} \tag{10}$$

$$\frac{di_{qr}}{dt} = -\frac{R_r}{\Upsilon} i_{qr} - \omega_r i_{dr} - \frac{M \omega_r}{\Upsilon L_s} \phi_{ds} + \frac{1}{\Upsilon} V_{qr} \tag{11}$$

with $\Upsilon = L_r(1 - \frac{M^2}{L_r L_s})$.

3. Fuzzy Logic-Based Control (FLC)

Fuzzy Logic Control is a strategy of control derived from fuzzy set theory, developed to handle systems that exhibit uncertainty, nonlinear behavior, and imprecision. In contrast to traditional controllers that depend heavily on accurate mathematical representations, FLC mimics human decision-making by analyzing approximate data conveyed via linguistic variables. This characteristic makes FLC especially advantageous for systems with time-varying parameters and dynamic operating environments, such as renewable energy and microgrid applications [34], [35]. The FLC was selected for its ability to handle the non-linear and uncertain behavior of DFIG-based WECS without relying on an exact model. A brief sensitivity analysis shows that moderate parameter variations have a limited impact on control performance, which confirms the robustness of the approach.

One of the main strengths of FLC is its flexibility and adaptability. Since it does not require an exact system model, it can easily adjust to changes in dynamic's system and external disturbances. This adaptability is highly valuable in power and energy systems, where fluctuations in load demand and generation are common [36], [37]. The general structure of a fuzzy logic controller is illustrated in Fig. 2, which consists of three sequential phases: fuzzification, inference, and defuzzification [38]. During the fuzzification process, precise numerical inputs are converted into fuzzy values represented by descriptive linguistic terms such as low, medium, or high. The inference system then utilizes a pre-established rule set, typically formulated as a collection of IF-THEN rules, to define the relationship between input data and control responses. Lastly, in the defuzzification phase, the fuzzy result is transformed into a clear control signal suitable for execution by the physical system [39], [40].

Fig. 3 presents the fuzzy sets along with the triangular membership functions (MFs) assigned to each signal. In this work, five MFs are adopted for both the input and output variables, namely NB (negative big), NM (negative medium), NS (negative small), Z (zero), PS (positive small), PM (positive medium), and PB (positive big). The MFs are arranged symmetrically around the origin, providing balanced representation for both positive and negative regions. The controller takes the error (e) and its rate of change ($\frac{de}{dt}$) as inputs, while the control increment ($\frac{du}{dt}$) serves as the output.

The fuzzy rule base is constructed using a set of *If–Then* logical rules. In the rule matrix (Table 1), the rows and columns correspond to the fuzzy sets of e and de/dt, while the body of the matrix specifies the output fuzzy set for du. With five membership functions per variable, the controller operates on a total of 49 rules, ensuring effective mapping between input conditions and control actions.

In the fuzzy logic framework, rule evaluation is performed using the fuzzy intervals of the variable μ, which yield corresponding output membership functions. These outputs are then translated into a crisp physical value of μ through the center of gravity (COG) defuzzification technique. This

approach determines the centroid of the fuzzy set by computing the weighted average of its area, as expressed in the following equation:

$$COG = \frac{\sum_k u_k\left(\delta\mu(k)\right) \cdot \mu(k)}{\sum_k u_k\left(\delta\mu(k)\right)} \tag{12}$$

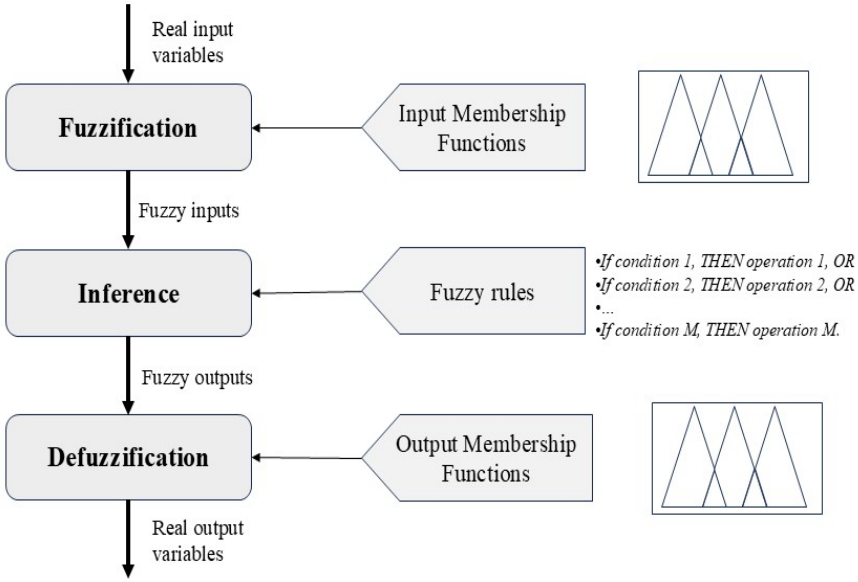

Fig. 2. Architecture of a Fuzzy Logic Control System

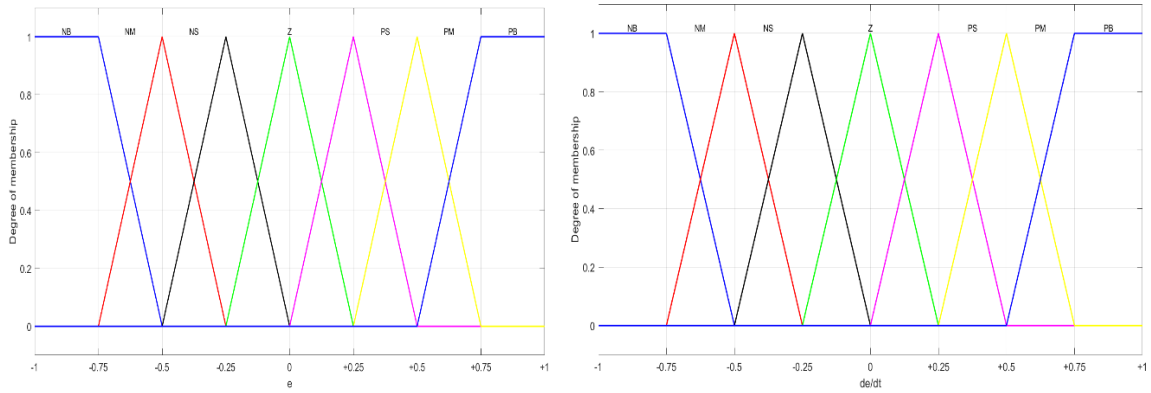

(a) (b)

Fig. 3. Membership functions of the proposed fuzzy controller: (a) error e; (b) derivative of error $\frac{de}{dt}$

Table 1. Rule matrix for fuzzy logic controller

de/dt	e						
	NB	**NM**	**NS**	**Z**	**PS**	**PM**	**PB**
NB	NB	NB	NB	NG	NM	NP	Z
NM	NB	NB	NB	NM	NP	Z	PP
NS	NB	NB	NM	NP	Z	PP	PM
Z	NB	NM	NP	Z	PP	PM	PG
PS	NM	NP	Z	PP	PM	PG	PG
PM	NP	NE	PP	PM	PG	PG	PG
PB	Z	PP	PM	PG	PG	PG	PG

4. Application of FLC in DFIG-Based WECS

4.1. MPPT algorithm

The power captured by WECS is highly dependent on the rotor speed of the generator. To maximize energy extraction, the turbine must operate at its optimal power point, which corresponds to the rotor speed that achieves peak aerodynamic efficiency. This is accomplished through a MPPT control strategy, which dynamically adjusts the reference rotor speed, ω_{ref}, to maintain optimal performance [41]-[43].

Among the various MPPT strategies, the Perturb and Observe (P&O) method is widely adopted due to its simplicity, robustness, and effectiveness. The P&O algorithm operates by introducing a small perturbation to the rotor speed and monitoring the resulting change in output power. If the power increases following the perturbation, the algorithm continues adjusting the speed in the same direction; otherwise, it reverses the perturbation. This iterative process allows the system to converge toward the maximum power point, even under fluctuating wind speeds [44], [45].

In this study, the P&O algorithm generates the optimal rotor speed reference, (ω_{ref}), which is tracked by the rotor-side converter within a back-to-back converter system. The flowchart of the algorithm is depicted in Fig. 4. At each sampling interval, the algorithm measures the current rotor speed and the corresponding output power, compares these values with their previous states, and determines whether to increment or decrement the reference speed by a predefined step size, ($\Delta\omega$). This adaptive approach ensures that the turbine operates close to the MPP, maximizing energy capture across a wide range of wind conditions.

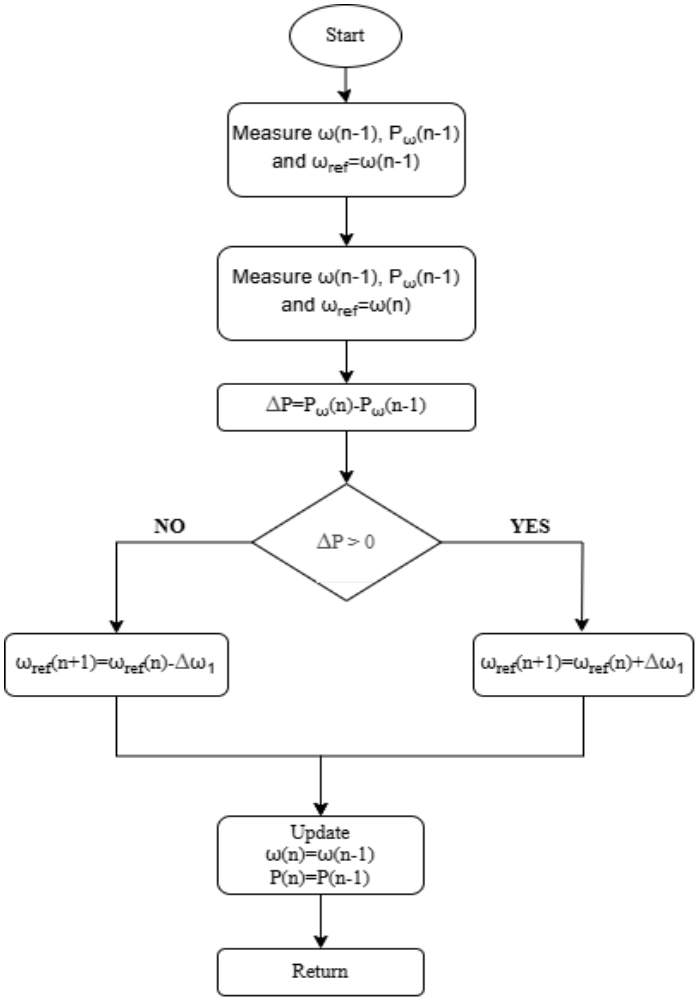

Fig. 4. Implementation of variable-step P&O MPPT strategy

4.2. RSC Control Method

The Rotor-Side Converter (RSC) plays a critical role in the operation of a DFIG -based wind energy conversion system. The RSC is primarily responsible for regulating the rotor currents of the DFIG to achieve two key objectives: Maximum Power Point Tracking (MPPT) through precise rotor speed control and independent reactive power management.

4.2.1. Speed control of DFIG using FLC

Implementing a fuzzy logic controller for speed regulation is essential to achieving MPPT and ensuring efficient power generation in wind turbines. The developed controller dynamically adjusts the speed to follow the reference signal speed which can provided by an MPPT algorithm. The controller evaluates the error signal ($e(\omega) = \omega_{ref} - \omega$) where ($\omega_{ref}$) is the optimal speed provided by the P&O algorithm, and (ω) is the actual rotor speed. Based on the proposed controller structure in Fig. 2, the MSF are illustrated in Fig. 3. The range of values for the variables $u(e(\omega))$ and $u(\delta e(\omega))$, where ($\delta e(\omega) = \frac{\Delta e(\omega)}{T_s}$), and ($T_s$) is the sampling time, is defined by the operating ranges of the system's inputs, in particular the error ($e(\omega)$). With this configuration, it is assured that the range encompasses all speed variations, enabling the FLC to maintain optimal performance and achieve effective MPPT across diverse wind speeds.

4.2.2. Stator reactive power control using FLC

In this part, the reactive power control is designed to regulate the reactive power exchanged between the GSC and the grid. As illustrated in Fig. 2, the controller applies a fuzzy logic approach to dynamically adjust the reactive power injected into the grid. The input variables to the controller are the reactive power error, defined as $e(Q_s) = Q_s - Q_{sref}$, which represents the deviation between the reference reactive power (Q_{sref}) and the measured grid-side reactive power (Q_s), and the rate of change of the error, expressed as $\delta e(Q_s) = \frac{\Delta e(Q_s)}{T_s}$, where T_s is the sampling period.

The membership functions, presented in Fig. 3, cover the full range of expected reactive power variations. By processing these inputs through fuzzy inference rules, the controller generates appropriate control actions, thereby achieving accurate and adaptive regulation of reactive power. This capability ensures stable operation under varying grid conditions, while also providing critical voltage support and meeting regulatory demands.

4.3. GSC Control Method

The GSC regulates the DC-link voltage to ensure seamless operation of the back-to-back converter system and controls the flow of active power to the grid. Additionally, it manages reactive power exchange to achieve power factor correction (PFC).

4.3.1. DC-link Voltage Control Using FLC

The primary objective of the GSC is to ensure precise synchronization of the currents with the grid voltage, while maintaining the DC-link voltage (V_{dc}) at a predefined reference value (V_{dc_ref}). As shown in Fig. 2, the fuzzy logic controller employs membership functions that are detailed in Fig. 3. The controller utilizes two input variables: the DC-link voltage error $e(V_{dc}) = V_{dc} - V_{dc\_ref}$, which represents the deviation between the reference and the actual DC-link voltage, and the rate of change of the error ($\delta e(V_{dc}) = \frac{\Delta e(V_{dc})}{T_s}$), where (T_s) represents the sampling-time. The discourse universe for these inputs is carefully determined to encompass the full operating range of the system. This guaranties that the MSF functions comprehensively cover DC-link voltage variations, enabling the fuzzy controller to deliver precise and effective responses.

4.3.2. Power Factor Correction Using FLC

The fuzzy logic controller for power factor correction is designed to regulate the reactive power exchange with the grid to meet specified reference values, ensuring compliance with grid codes and

supporting voltage stability. As depicted in Fig. 2, the controller employs a fuzzy logic approach to dynamically adjust the reactive power output. The controller receives as input variables the reactive power error $e(Q_g) = Q_g - Q_{gref}$, defined as the difference between the reference reactive power (Q_{ref}) and the actual reactive power (Q), and the rate of change of the error ($\delta e(Q_g) = \frac{\Delta e(Q_g)}{T_s}$), where ($T_s$) is the sampling time. The membership functions, detailed in Fig. 3 and configured depending on the boundaries of the system's operation to ensure comprehensive coverage of reactive power variations. This enables the fuzzy controller to provide precise and adaptive control, maintaining optimal reactive power delivery and enhancing grid stability.

5. Results and Discussions

The fuzzy logic controller, designed in Section 4, was evaluated through simulation within the MATLAB/Simulink environment (Fig. 5). The simulated DFIG-based WECS considers the overall scheme described in Fig. 1, using the electromechanical parameters summarized in Table 2. The implemented control strategy includes the MPPT algorithm, and the fuzzy logic controllers, which are applied through the rotor-side and grid-side converters. The simulation setup conditions were defined by variations in wind speed profiles in order to evaluate the dynamic performance of the proposed FLC scheme. To this end, two types of wind speed profiles were considered: step variations and a random (realistic) profile.

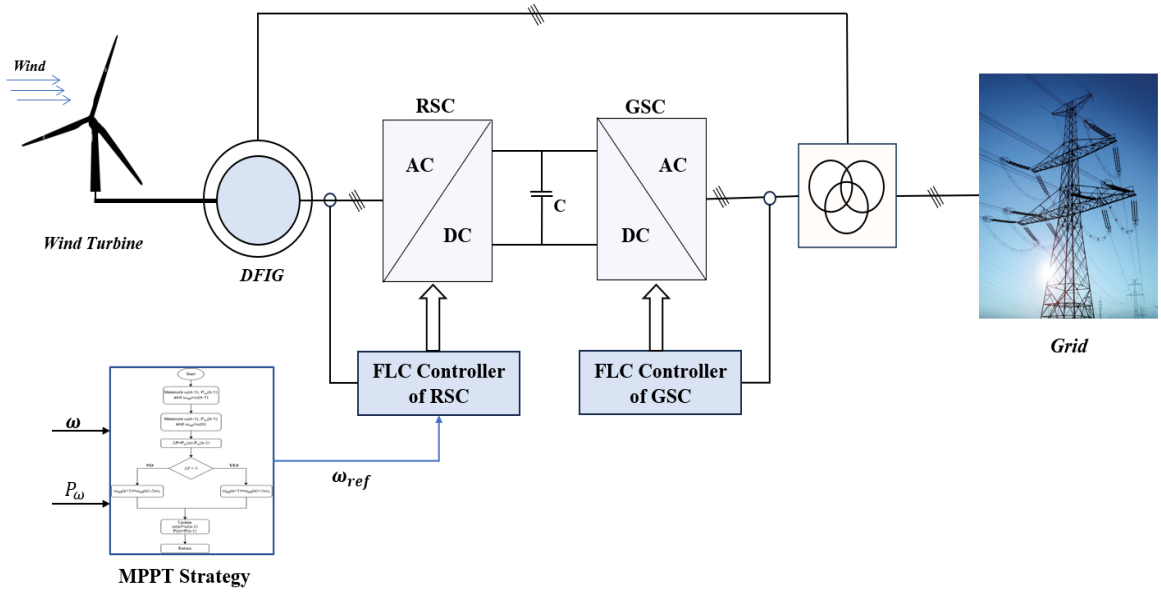

Fig. 5. Schematic representation of a grid-connected DFIG-based WECS

5.1. Performance Under Step Wind Speed Variations

In the first scenario, step changes in wind speed were applied to the system in order to assess the controller's ability to track the maximum power point and regulate the system variables under abrupt operating conditions (Fig. 6). This test highlights the transient response, stability, and adaptability of the proposed fuzzy logic controller when subjected to sudden variations in wind speed.

Fig. 7 illustrates the rotor speed of the DFIG and its reference provided by the MPPT algorithm. It is clear that the rotor speed effectively tracks its reference within a short time, demonstrating the responsiveness of the control system and ensuring optimal power extraction under varying conditions. The right-hand plot provides a zoomed-in view, highlighting the precise alignment between the actual rotor speed and the reference over a smaller time scale.

Table 2. Parameters of the DFIG-Based WECS model

Parameter	Symbol	Value	Unit
DFIG Parameters			
Stator resistance	R_s	0.35	Ω
Rotor resistance	R_r	0.73	Ω
Stator inductance	L_s	0.047	H
Rotor inductance	L_r	0.061	H
Mutual inductance	M	0.067	H
Pole pairs	p	2	–
Generator inertia	J_g	0.3	kg·m²
Generator friction	f_g	6.12×10^{-3}	N·m·s
Wind Turbine Parameters			
Air density	ρ	1.25	kg/m³
Blade radius	R	5	M
Gearbox ratio	G	5	–
Turbine inertia	J_t	0.037	kg·m²
Turbine friction	f_t	0.029	N·m·s
Grid Side Parameters			
Grid resistance	R_g	0.02	Ω
Grid inductance	L_g	0.11	H
Grid angular frequency	ω_g	314	rad/s
Grid voltage	E_g	230	V

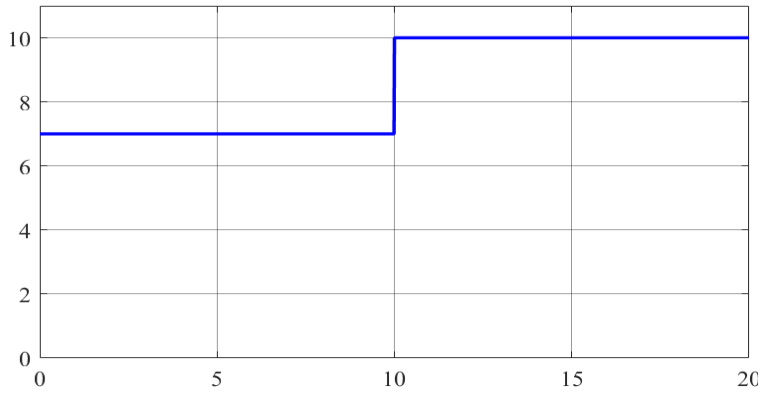

Fig. 6. Wind speed variation

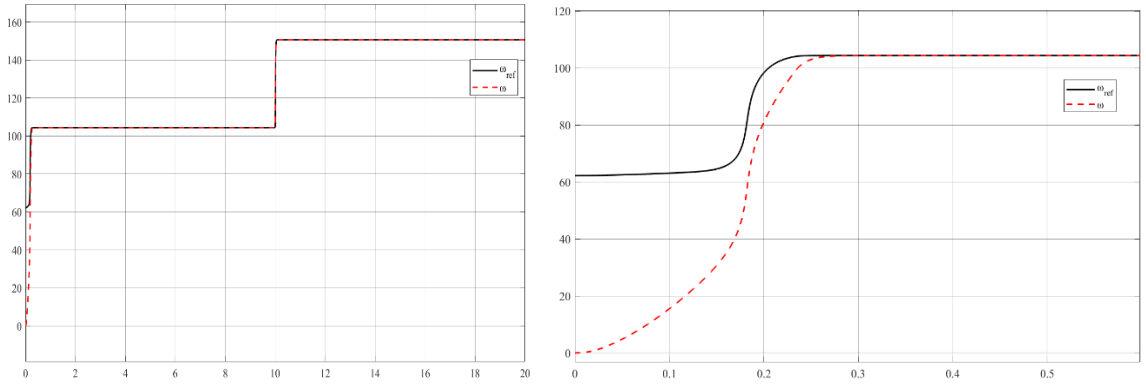

(a) Rotor speed (b) Zoom

Fig. 7. Rotor speed of the DFIG and its reference

Fig. 8-(a), the stator active power is depicted, showing a stable output that remains consistent over time. Fig. 8-(b) represents the stator reactive power, which is maintained at a near-zero level, reflecting the system's ability to minimize reactive power flow and enhance overall efficiency. Fig. 9

highlights the effectiveness of the proposed control strategy for the GSC. In Fig. 9-(a), the DC-link voltage Vdc is well-regulated and swiftly stabilizes following changes in operating conditions, such as variations in speed reference. Fig. 9-(b) verifies the unity power factor, showing that the grid voltage and current are in phase, ensuring high-quality current injection into the power grid.

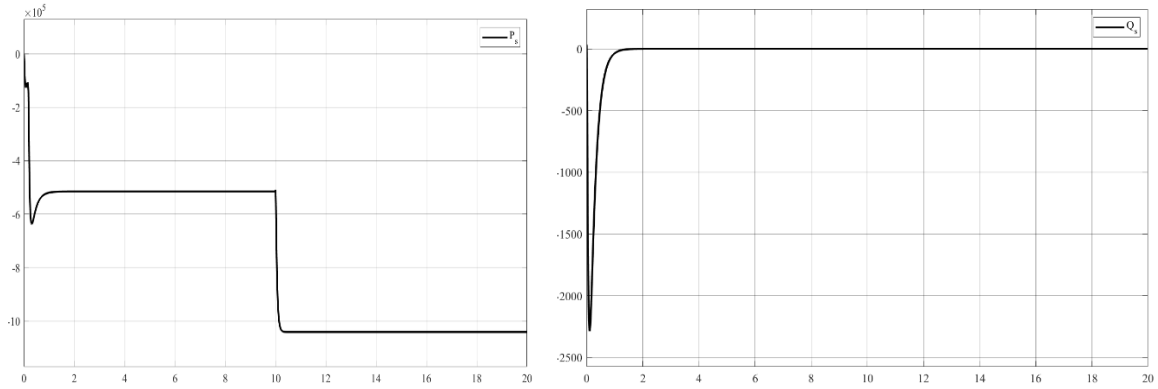

(a) Active power (b) Reactive power

Fig. 8. The active and reactive power of stator

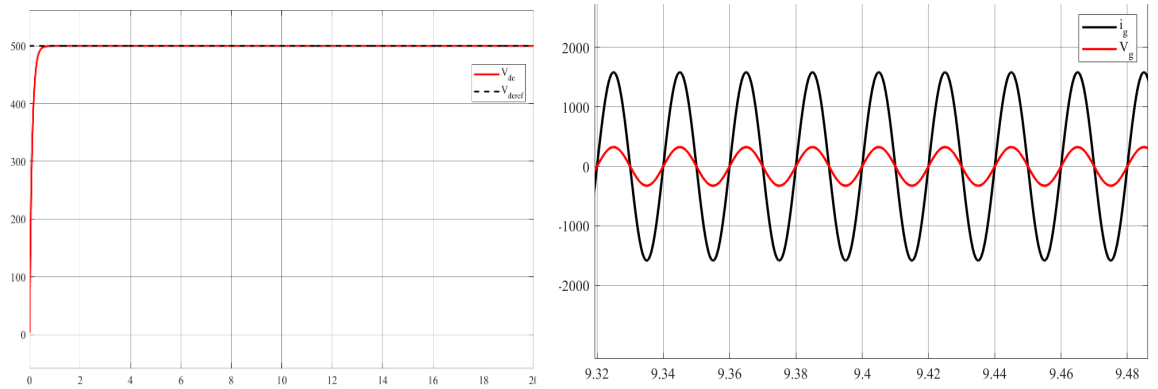

(a) The DC-Link voltage (b) Verification of unity power factor

Fig. 9. The performance of the proposed control for the GSC

5.2. Performance Under Random Wind Speed Profile

In the second scenario, a stochastic (random) wind speed profile was introduced to emulate realistic operating conditions of a wind turbine (Fig. 10). This test aims to demonstrate the robustness and reliability of the proposed fuzzy logic controller under practical wind fluctuations. The obtained results illustrate the effectiveness of the controller in maintaining stable operation, ensuring efficient power extraction, and regulating reactive power and DC-link voltage despite the intermittency of wind speed.

Fig. 11 displays the rotor speed of the DFIG alongside its reference under random wind speed conditions. The rotor speed effectively follows its reference with notable responsiveness, as highlighted in the zoomed-in (Fig. 11-(b)), reflecting the control system's ability to adapt quickly to fluctuating wind inputs. In Fig. 12-(a), the active power exhibits dynamic fluctuations, aligning with the changing wind conditions. Fig. 12-(b) shows the reactive power remaining near zero, demonstrating the system's capability to minimize reactive power flow and enhance efficiency.

In Fig. 13-(a), the DC-link voltage V_{dc} is effectively maintained at its reference value V_{dcref} with rapid stabilization following initial adjustments. Fig. 13-(b) verifies the unity power factor, where the

grid voltage and current are in phase, as indicated by the highlighted zoom-in, confirming effectiveness of the proposed controller under random wind speed conditions.

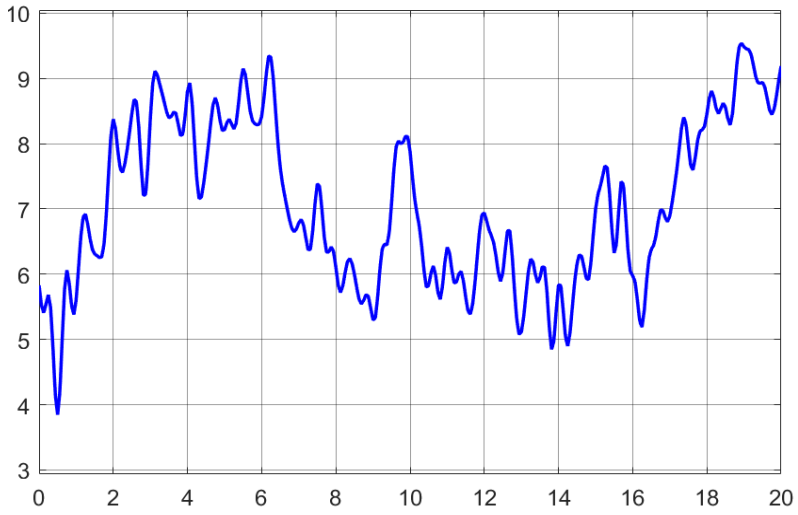

Fig. 10. Wind speed variation

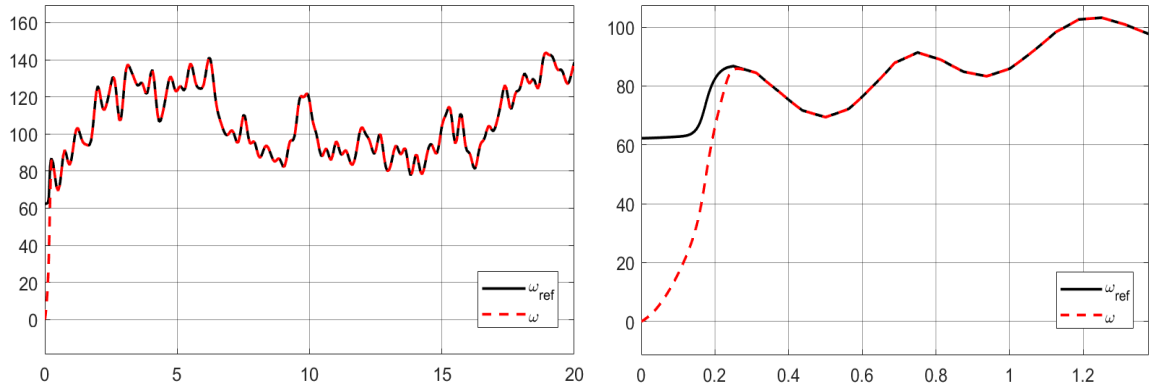

(a) Rotor speed (b) Zoom

Fig. 11. Rotor speed of the DFIG and its reference

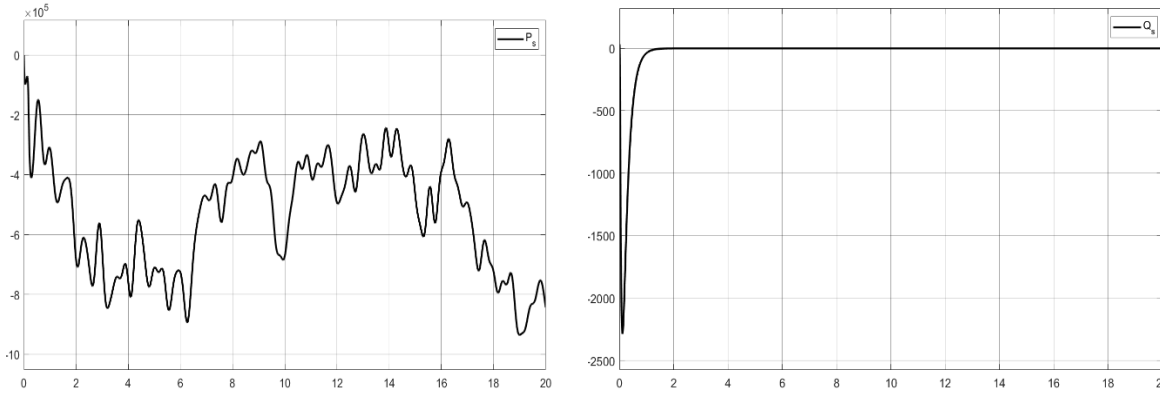

(a) Active power (b) Reactive power

Fig. 12. The active and reactive power of stator

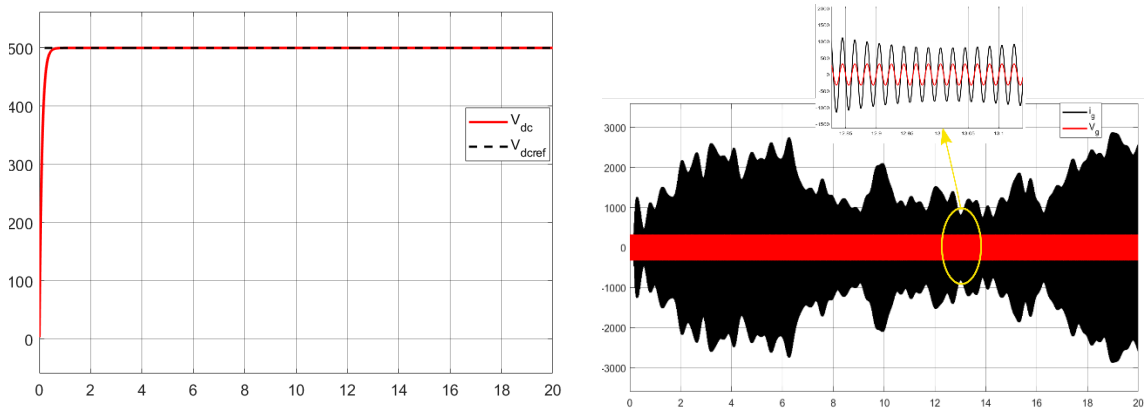

(a) The DC-Link voltage (b) Verification of unity power factor

Fig. 13. The performance of the proposed control for the GSC

5.3. Comparative Performance Analysis

To consolidate the validation of the control strategy, we conducted a rigorous comparative study pitting the proposed FLC against a conventional PI controller, subjecting them to the same wind speed variations. The analysis focused on essential performance criteria: settling time, overshoot, steady-state error, and robustness to disturbances. Table 3 summarizes these results, unequivocally demonstrating that the FLC offers superior dynamics (faster response, lower overshoot, and increased accuracy in the steady state) compared to the PI controller. Finally, the FLC's ability to maintain stable operation despite rapid wind fluctuations confirms its robustness and relevance for operational integration into DFIG-based WECS.

Table 3. Comparative performance between the PI controller and the proposed FLC

Performance Metric	PI Controller	Proposed FLC	Observation
Settling time of rotor speed	≈ 1 s	≈ 0.3 s	50% faster dynamic response
Overshoot in rotor speed	5 %	2 %	FLC reduces overshoot significantly
Steady-state error	0.7 %	0 %	Perfect tracking achieved
Active power ripple	±5 %	±1.5 %	Smoother power response
Reactive power regulation	Slight oscillations	Stable (Q ≈ 0)	Improved voltage/power factor control
DC-link voltage variation	±20 V	±5 V	Enhanced voltage stability
Power factor at grid side	0.995	≈ 1.000	Unity power factor maintained
Robustness to wind variation (7–10 m/s)	Moderate degradation	Stable performance	FLC adapts better to nonlinear conditions
Computational complexity	Low	Moderate	Slightly higher due to rule base but acceptable

The complete implementation procedure of the proposed advanced control method, encompassing the integrated P&O MPPT strategy and the FLC design, is recapitulated in the structured flowchart shown in Fig. 14.

6. Conclusion

In conclusion, this paper has comprehensively investigated the control challenges associated with wind energy conversion systems utilizing doubly fed induction generators (DFIGs) driven by advanced converters, particularly the AC/DC/AC converter. This focus on the new generation of converters, with their ability of bidirectional power flow and enhances the waveform quality and ensuring efficient energy conversion. The paper analyzed the performance of a wind turbine integrated with a DFIG powered by a buck-to-buck converter employing MPPT techniques based on P&O algorithm. The evaluation, conducted in the dq reference frame, demonstrated the effectiveness of the proposed control scheme in optimizing power generation under varying wind conditions, The

proposed control strategy is evaluated under both step-change and random wind speed profiles to assess its effectiveness across diverse operating conditions. The successful implementation and validation of the control strategy through simulation results using MATLAB/Simulink reaffirm the viability and robustness of the proposed approach.

For future research directions, it is important to acknowledge that implementing multiple FLCs in real-time may increase computational complexity and lead to a potential rule-base expansion, which can complicate the tuning and maintenance process in practical applications. Therefore, future work will focus on integrating Artificial Intelligence (AI)-based MPPT algorithms into the control design of WECS, as these techniques can intelligently manage the rule-base, reduce manual tuning effort, and ensure optimal power extraction under varying wind conditions. Experimental validation will also be pursued to further substantiate the feasibility and robustness of the proposed approach.

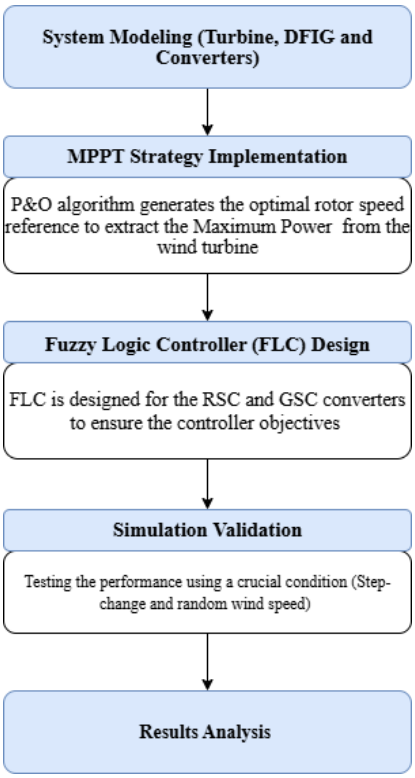

Fig. 14. Comparative performance between the PI controller and the proposed FLC

Author Contribution: All authors contributed equally to the main contributor to this paper. All authors read and approved the final paper.

Conflicts of Interest: The authors declare no conflict of interest.

References

[1] J. Tian, S. A. Culley, H. R. Maier, and A. C. Zecchin, "Is renewable energy sustainable? Potential relationships between renewable energy production and the Sustainable Development Goals," *npj Climate Action*, vol. 3, no. 1, p. 35, May 2024, https://doi.org/10.1038/s44168-024-00120-6.

[2] F. Blouh, B. Boujidi, and M. Bezza, "Wind energy conversion system based on DFIG using three-phase AC-AC matrix converter," *International Journal of Power Electronics and Drive Systems*, vol. 14, no. 3, p. 1865, Sep. 2023, https://doi.org/10.11591/ijpeds.v14.i3.pp1865-1875.

[3] B. En-Nouaary, R. Beniaich, and A. Hmioui, "Prioritizing sustainability of renewable energy projects in Morocco," *International Journal of Energy Sector Management*, vol. 19, no. 3, pp. 612–631, Nov. 2024, https://doi.org/10.1108/IJESM-06-2024-0014.

[4] R. Benbba, M. Barhdadi, A. Ficarella, G. Manente, M. P. Romano, N. El Hachemi, A. Barhdadi, A. Al-Salaymeh, and A. Outzourhit, "Solar energy resource and power generation in Morocco: Current situation, potential, and future perspective," *Resources*, vol. 13, no. 10, p. 140, 2024, https://doi.org/10.3390/resources13100140.

[5] F. Blouh, M. Bezza, and I. El Myasse, "Modeling and control of an aerogenerator utilizing DFIG and direct matrix converter technology," in *2024 4th International Conference on Innovative Research in Applied Science, Engineering and Technology (IRASET)*, May 2024, pp. 1-6, https://doi.org/10.1109/IRASET60544.2024.10548696.

[6] J. D. Tan, C. C. W. Chang, M. A. S. Bhuiyan, K. N. Minhad, and K. Ali, "Advancements of wind energy conversion systems for low-wind urban environments: A review," *Energy Reports*, vol. 8, pp. 3406–3414, Nov. 2022, https://doi.org/10.1016/j.egyr.2022.02.153.

[7] I. El Myasse, A. El Magri, A. Watil, A. Mansouri, M. Kissaoui, H. Ouabi, and F. E. Blouh, "Enhancing wind power plant integration using a T-NPC converter with DR-HVDC transmission systems," *IFAC-PapersOnLine*, vol. 58, no. 13, pp. 472–477, 2024, https://doi.org/10.1016/j.ifacol.2024.07.527.

[8] V. C. Ganti, B. Singh, S. K. Aggarwal, and T. C. Kandpal, "DFIG-based wind power conversion with grid power leveling for reduced gusts," *IEEE Transactions on Sustainable Energy*, vol. 3, no. 1, pp. 12–20, Jan. 2012, https://doi.org/10.1109/TSTE.2011.2170862.

[9] K. B. Tawfiq, A. S. Mansour, H. S. Ramadan, M. Becherif, and E. E. El-Kholy, "Wind energy conversion system topologies and converters: Comparative review," *Energy Procedia*, vol. 162, pp. 38-47, Apr. 2019, https://doi.org/10.1016/j.egypro.2019.04.005.

[10] A. A. Chhipa, P. Chakrabarti, V. Bolshev, T. Chakrabarti, G. Samarin, A. N. Vasilyev, S. Ghosh, and A. Kudryavtsev, "Modeling and control strategy of wind energy conversion system with grid-connected doubly-fed induction generator," *Energies*, vol. 15, no. 18, p. 6694, 2022, https://doi.org/10.3390/en15186694.

[11] X. Liu, Z. Zhang, Y. Liu, L. Yuan, M. Su, F. Zhou, C. Li, J. Liu, X. Zhang, and P. Wang, "Fault current multi-stages calculation method for DFIG-based wind farms with whole fault process attributes under asymmetrical grid fault conditions," *IEEE Transactions on Sustainable Energy*, vol. 15, no. 4, pp. 2361-2379, 2024, https://doi.org/10.1109/TSTE.2024.3418147.

[12] M. Boutoubat, L. Mokrani, and M. Machmoum, "Control of a wind energy conversion system equipped by a DFIG for active power generation and power quality improvement," *Renewable Energy*, vol. 50, pp. 378-386, Feb. 2013, https://doi.org/10.1016/j.renene.2012.06.058.

[13] S. Cheng, H. Wang, Y. Zheng, F. Zheng, Z. Chen, H. Bevrani, and J. Yang, "Comparison analysis for inter-area oscillation suppression of DFIG based on POD applied to RSC and GSC," *Electrical Engineering*, vol. 107, no. 11, pp. 14587-14600, Nov. 2025, https://doi.org/10.1007/s00202-025-03281-7.

[14] G. Kambam, P. Somasundaram, and G. V. Swaminathan, "Design of GSC and RSC controllers for DFIG using GA based optimization algorithm," in *2023 9th International Conference on Electrical Energy Systems (ICEES)*, Mar. 2023, pp. 210-215, https://doi.org/10.1109/ICEES57979.2023.10110288.

[15] R. Patel, F. Hafiz, A. Swain, and A. Ukil, "Nonlinear rotor side converter control of DFIG based wind energy system," *Electric Power Systems Research*, vol. 198, p. 107358, Sep. 2021, https://doi.org/10.1016/j.epsr.2021.107358.

[16] S. Bhattacharyya, S. Puchalapalli, and B. Singh, "Operation of grid-connected PV-battery-wind driven DFIG based system," *IEEE Transactions on Industry Applications*, vol. 58, no. 5, pp. 6448-6458, Sep. 2022, https://doi.org/10.1109/TIA.2022.3181124.

[17] F. Amrane, B. Francois, and A. Chaiba, "Experimental investigation of efficient and simple wind-turbine based on DFIG-direct power control using LCL-filter for stand-alone mode," *ISA Transactions*, vol. 125, pp. 631-664, Jun. 2022, https://doi.org/10.1016/j.isatra.2021.07.008.

[18] M. M. Alhato and S. Bouallègue, "Direct power control optimization for doubly fed induction generator-based wind turbine systems," *Mathematical and Computational Applications*, vol. 24, no. 3, p. 77, Sep. 2019, https://doi.org/10.3390/mca24030077.

[19] H. Benbouhenni and N. Bizon, "Advanced direct vector control method for optimizing the operation of a double-powered induction generator-based dual-rotor wind turbine system," *Mathematics*, vol. 9, no. 19, p. 2403, Jan. 2021, https://doi.org/10.3390/math9192403.

[20] R. Hiremath and T. Moger, "Modified super twisting algorithm based sliding mode control for LVRT enhancement of DFIG driven wind system," *Energy Reports*, vol. 8, pp. 3600-3613, Nov. 2022, https://doi.org/10.1016/j.egyr.2022.02.235.

[21] O. Beik and A. S. Al-Adsani, "Active and passive control of a dual rotor wind turbine generator for DC grids," *IEEE Access*, vol. 9, pp. 1987-1995, 2021, https://doi.org/10.1109/ACCESS.2020.3047267.

[22] C. Chatri, M. Labbadi, M. Ouassaid, K. Elyaalaoui, and Y. El Houm, "Design and implementation of finite-time control for speed tracking of permanent magnet synchronous motors," *IEEE Control Systems Letters*, vol. 7, pp. 721-726, 2023, https://doi.org/10.1109/LCSYS.2022.3221719.

[23] C. Chatri, M. Ouassaid, M. Labbadi, and Y. Errami, "Integral-type terminal sliding mode control approach for wind energy conversion system with uncertainties," *Computers and Electrical Engineering*, vol. 99, p. 107775, Apr. 2022, https://doi.org/10.1016/j.compeleceng.2022.107775.

[24] C. Chatri, M. Labbadi, and M. Ouassaid, "Improved high-order integral fast terminal sliding mode-based disturbance-observer for the tracking problem of PMSG in WECS," *International Journal of Electrical Power & Energy Systems*, vol. 144, p. 108514, Jan. 2023, https://doi.org/10.1016/j.ijepes.2022.108514.

[25] H. Kong, J. He, Y. Liu, P. Cheng, and J. Ma, "Improved direct power control of doubly fed induction generator without phase-locked loop," in *2020 IEEE Sustainable Power and Energy Conference (iSPEC)*, Nov. 2020, pp. 199-204, https://doi.org/10.1109/iSPEC50848.2020.9351036.

[26] H. Benbouhenni, F. Mehedi, and L. Soufiane, "New direct power synergetic-SMC technique based PWM for DFIG integrated to a variable speed dual-rotor wind power," *Automatika: časopis za automatiku, mjerenje, elektroniku, računarstvo i komunikacije*, vol. 63, no. 4, pp. 718-731, Jun. 2022, https://doi.org/10.1080/00051144.2022.2065801.

[27] F. Echiheb, Y. Ihedrane, B. Bossoufi, M. Bouderbala, S. Motahhir, M. Masud, S. Aljahdali, and M. ElGhamrasni, "Robust sliding-backstepping mode control of a wind system based on the DFIG generator," *Scientific Reports*, vol. 12, no. 1, p. 11782, Jul. 2022, https://doi.org/10.1038/s41598-022-15960-7.

[28] H. Benbouhenni and N. Bizon, "A new direct power control method of the DFIG-DRWT system using neural PI controllers and four-level neural modified SVM technique," *Journal of Applied Research and Technology*, vol. 21, no. 1, pp. 36-55, 2023, https://doi.org/10.22201/icat.24486736e.2023.21.1.2171.

[29] H. Gasmi, S. Mendaci, S. Laifa, W. Kantas, and H. Benbouhenni, "Fractional-order proportional-integral super twisting sliding mode controller for wind energy conversion system equipped with doubly fed induction generator," *Journal of Power Electronics*, vol. 22, no. 8, pp. 1357-1373, Aug. 2022, https://doi.org/10.1007/s43236-022-00430-0.

[30] R. K. Pachauri and Y. K. Chauhan, "Mechanical control methods in wind turbine operations for power generation," *Journal of Automation and Control Engineering*, vol. 2, no. 3, pp. 214-220, 2014, https://doi.org/10.12720/joace.2.3.214-220.

[31] A. Petersson, T. Thiringer, L. Harnefors, and T. Petru, "Modeling and experimental verification of grid interaction of a DFIG wind turbine," *IEEE Transactions on Energy Conversion*, vol. 20, no. 4, pp. 878-886, Dec. 2005, https://doi.org/10.1109/TEC.2005.853750.

[32] A. Luna, F. K. A. Lima, D. Santos, P. Rodriguez, E. H. Watanabe, and S. Arnaltes, "Simplified modeling of a DFIG for transient studies in wind power applications," *IEEE Transactions on Industrial Electronics*, vol. 58, no. 1, pp. 9-20, Jan. 2011, https://doi.org/10.1109/TIE.2010.2044131.

[33] L. Xu and Y. Wang, "Dynamic modeling and control of DFIG-based wind turbines under unbalanced network conditions," *IEEE Transactions on Power Systems*, vol. 22, no. 1, pp. 314-323, 2007, https://doi.org/10.1109/TPWRS.2006.889113.

[34] A. El Azzab, A. El Magri, I. El Myasse, and R. Lajouad, "Efficient energy management using fuzzy logic control in a gym microgrid with stationary bikes, PV generation, and battery storage systems," *Scientific African*, vol. 28, p. e02674, Jun. 2025, https://doi.org/10.1016/j.sciaf.2025.e02674.

[35] B. E. Elnaghi, A. M. Ismaiel, F. El Sayed Abdel-Kader, M. N. Abelwhab, and R. H. Mohammed, "Validation of energy valley optimization for adaptive fuzzy logic controller of DFIG-based wind turbines," *Scientific Reports*, vol. 15, no. 1, p. 711, Jan. 2025, https://doi.org/10.1038/s41598-024-82382-y.

[36] K. El Mezdi, A. El Magri, A. Watil, I. El Myasse, and L. Bahatti, "Integrated control and energy flow management for hybrid grid-connected photovoltaic/wind systems with battery storage using fuzzy logic controllers," *IFAC-PapersOnLine*, vol. 58, no. 13, pp. 442-447, Jan. 2024, https://doi.org/10.1016/j.ifacol.2024.07.522.

[37] K. E. Mezdi, A. E. Magri, L. Bahatti, N. Elaadouli, and I. E. Myasse, "Integrated control and energy flow management in hybrid stand-alone photovoltaic/wind systems with battery storage using fuzzy logic controllers," in *2024 4th International Conference on Innovative Research in Applied Science, Engineering and Technology (IRASET)*, May 2024, pp. 1-6, https://doi.org/10.1109/IRASET60544.2024.10548900.

[38] T. Samavat, M. Nazari, M. Ghalehnoie, M. A. Nasab, M. Zand, P. Sanjeevikumar, and B. Khan, "A comparative analysis of the Mamdani and Sugeno fuzzy inference systems for MPPT of an islanded PV system," *International Journal of Energy Research*, vol. 2023, no. 1, p. 7676113, 2023, https://doi.org/10.1155/2023/7676113.

[39] R. Vidal-Martínez, J. R. García-Martínez, R. Rojas-Galván, J. M. Álvarez-Alvarado, M. Gozález-Lee, and J. Rodríguez-Reséndiz, "A review of Mamdani, Takagi-Sugeno, and Type-2 fuzzy controllers for MPPT and power management in photovoltaic systems," *Technologies*, vol. 13, no. 9, p. 422, Sep. 2025, https://doi.org/10.3390/technologies13090422.

[40] D. K. Jain, S. Neelakandan, T. Veeramani, S. Bhatia, and F. H. Memon, "Design of fuzzy logic based energy management and traffic predictive model for cyber physical systems," *Computers and Electrical Engineering*, vol. 102, p. 108135, Sep. 2022, https://doi.org/10.1016/j.compeleceng.2022.108135.

[41] M. Salman, S. A. R. Kashif, M. S. Fakhar, A. Rasool, and A. S. Hussen, "Optimizing power generation in a hybrid solar wind energy system using a DFIG-based control approach," *Scientific Reports*, vol. 15, no. 1, p. 10550, Mar. 2025, https://doi.org/10.1038/s41598-025-95248-8.

[42] S. Karad and R. Thakur, "Recent trends of control strategies for doubly fed induction generator based wind turbine systems: A comparative review," *Archives of Computational Methods in Engineering*, vol. 28, no. 1, pp. 15-29, Jan. 2021, https://doi.org/10.1007/s11831-019-09367-3.

[43] E. Bekiroglu and M. D. Yazar, "MPPT control of grid connected DFIG at variable wind speed," *Energies*, vol. 15, no. 9, p. 3146, Jan. 2022, https://doi.org/10.3390/en15093146.

[44] M. K. Saifullah, E. Jahan, and M. N. Uddin, "MPPT control for standalone wind energy conversion system: Integrating hybrid P&O; ANN with voltage-lift boost converter," in *2024 7th International Conference on Development in Renewable Energy Technology (ICDRET)*, Mar. 2024, pp. 1-6, https://doi.org/10.1109/ICDRET60388.2024.10503626.

[45] B. Naima, B. Belkacem, T. Ahmed, H. Benbouhenni, B. Riyadh, S. Heroual, S. Zaidi, Z. M. S. Elbarbary, and S. A. Mohammed, "Enhancing MPPT optimization with hybrid predictive control and adaptive P&O for better efficiency and power quality in PV systems," *Scientific Reports*, vol. 15, no. 1, p. 24559, Jul. 2025, https://doi.org/10.1038/s41598-025-10335-0.